Journal of Nuclear Materials 389 (2009) 191–196

Contents lists available at ScienceDirect

Journal of Nuclear Materials

journal homepage: www.elsevier.com/locate/jnucmat

The phase state at high temperatures in the MOX–SiO_2 system

S. Nakamichi [a,*], M. Kato [a], T. Sunaoshi [b], T. Uchida [a], K. Morimoto [a], M. Kashimura [a], Y. Kihara [a]

[a] Nuclear Fuel Cycle Engineering Laboratories, Japan Atomic Energy Agency, 4-33, Muramatsu, Tokai-mura, Naka-gun, Ibaraki 319-1194, Japan
[b] Inspection Development Company, 4-33, Tokai-mura, Naka-gun, Ibaraki 319-1194, Japan

A B S T R A C T

Influence of impurity Si on microstructure in a plutonium and uranium mixed oxide (MOX), which is used for fast breeder reactor fuel, was investigated, and phase state in 25% SiO_2 – $(U_{0.7}Pu_{0.3})O_2$ was observed as a function of oxygen chemical potential. Compounds composed of Pu and Si with other elements were observed at grain boundaries of the MOX parent phase in the specimens after annealing. These compounds were not observed in the grain interior and the MOX phase was not affected significantly by impurity Si. It was found that the compounds tended to form more observably with decreasing O/M ratio and with increasing annealing temperatures.

1. Introduction

The Japan Atomic Energy Agency has developed plutonium and uranium mixed oxide (MOX) fuels containing minor actinides (MA) as a fuel for advanced fast breeder reactors [1]. As a part of the development, a short-term irradiation test was carried out in the experimental fast reactor *Joyo*, and then the microstructures were observed on a cross-section of the irradiated pellets in a post irradiation examination. A small amount of melted (Pu,Si)-rich phase was observed at the edge of the center hole of the fuel pellets [2,3]. Impurity Si in the fuel was found to cause the formation of the (Pu,Si)-rich phase. Silicon is thought to be introduced into the raw materials during ball milling to adjust the Pu content in MOX fuels, because Si rubber is used as the lining of the milling pot. The content of Si in the pellets was within their fabricating specification.

In previous investigations, the influence of SiO_2 on microstructures in UO_2 was studied to obtain pellets with a larger grain size for development of high-burn up fuel. Such pellets were expected to reduce the release rate of FP gases because of a longer path for these gases to reach grain boundaries [4]. The phase diagram in the UO_2–SiO_2 system has been studied by Lungu and Beleuta [5]. They found that a liquid phase appeared above 1973 K and the liquidus temperature decreased with increasing SiO_2 content. None of the compounds consisting of U and Si were observed. However, the influence of Si on the microstructure in MOX is not understood yet, though the amount of Si in MOX is not negligible.

In addition, attention must be paid to the oxygen-to-metal (O/M) ratio of the MOX fuel. It is well known that properties of MOX, such as melting temperature and thermal conductivity, are dependent on the O/M ratio [6–9]. For example, the melting point of MOX increases with decreasing O/M ratio. Because the oxygen chemical potential of MOX decreases with decreasing O/M ratio, a decrease in the O/M ratio of MOX fuels could change the phase stability in the MOX–SiO_2 system. It is important for fuel design to determine the operating temperature by studying the phase stability in the MOX fuel as a function of the O/M ratio.

In this article, therefore, particular attention is paid to the influence of SiO_2 on the microstructure in MOX at high temperatures between the sintering temperature and the operating temperature of fuel material as a function of the O/M ratio.

2. Experimental

Powders of MOX and SiO_2 were used as raw materials. The MOX powder containing 30% Pu was prepared by a microwave co-conversion. These powders were mixed to the ratio of MOX to SiO_2 as 3:1 in mol fraction (MOX containing 25% SiO_2). The mixed powder was granulated and then pressed into pellets. In this process, lubricant was sprayed directly on the surface of the die before pressing. As a pre-sintering process, the samples were annealed at 1123 K for 5 h in an atmosphere at an oxygen potential of −414 kJ/mol controlled by a gas mixture of Ar and 5% H_2 with added moisture. The content of lubricant in a green pellet was very small, so it could be eliminated by the pre-sintering. Thereafter, the samples were sintered at 1823 K for 3 h in an atmosphere at an oxygen potential of −384 kJ/mol. These samples were annealed at 1973 K for 2 h (heat treatment 1) at three different oxygen potentials, −360, −405, and −435 kJ/mol, controlled by the ratio of H_2 to H_2O. After annealing, the samples were mechanically polished with waterproof paper, and buff-polished with alumina particles of 1 μm. Finally the samples were etched using an ion beam and were analyzed with an X-ray diffractometer (XRD: Rigaku

* Corresponding author. Tel.: +81 29 282 1111; fax.: +81 29 282 9473.
E-mail address: nakamichi.shinya@jaea.go.jp (S. Nakamichi).

0022-3115/$ - see front matter © 2009 Elsevier B.V. All rights reserved.
doi:10.1016/j.jnucmat.2009.01.028

RINT-1100), an optical microscope and an electron probe micro analyzer (EPMA: JEOL JXA8800).

The samples heated at 1973 K were annealed at 2273 K or 2673 K for 5 min (heat treatment 2) by induction heating. In this annealing, the samples were encapsulated into W capsules and the capsules were sealed in a vacuum by electron beam welding, this ensured that the O/M ratio of samples controlled by annealing at 1973 K (heat treatment 1) should be maintained. After heating, the samples were removed from the capsules and analyzed with an optical microscope, SEM (Hitachi S4300) and EPMA. Fig. 1 presents a flowchart for the experimental procedures of this work. The heating conditions are shown in Table 1.

3. Results and discussion

3.1. Effect of oxygen potential atmosphere on microstructure heated at 1973 K (heat treatment 1)

The XRD measurements were made in the range of 2θ from 10° to 145° for the samples annealed at 1973 K for 2 h and three different oxygen potentials: (a) −435 kJ/mol, (b) −405 kJ/mol, and (c) −360 kJ/mol. Fig. 2 shows XRD patterns due to Cu Kα1 magnifying the range of 2θ from 120° to 130°. The XRD peaks shifted to the low angle side with decreasing oxygen potential in the annealing atmosphere, which indicated that the lattice parameter of the sample increased with decreasing oxygen potential. The lattice parameters and the measured O/M ratios are summarized in Table 2. The former were determined by the Rieitveld method using XRD patterns. Because the solubility of SiO_2 in uranium dioxide with the same fluorite structure as MOX is low [10] and the lattice parameter of MOX depends on the O/M ratio, the O/M ratio was determined from the lattice parameter assuming that the influence of SiO_2 on the lattice parameter of MOX phase was negligible. The samples annealed at 1973 K with different oxygen potentials are found to have different O/M ratios ranging from 1.95 to 1.99.

Fig. 1. Experimental flow of this work.

Table 1
Heating conditions for each specimen.

Sample	Heat treatment 1			Heat treatment 2	
	Temperature (K)	Hold time (min)	Oxygen potential (kJ/mol)	Temperature (K)	Hold time (min)
(a)	1973	120	−435	–	–
(b)			−405	–	–
(c)			−360	–	–
(d)			−435	2273	5
(e)			−405	2273	
(f)			−360	2273	
(g)			−435	2673	
(h)			−405	2673	
(i)			−360	2673	

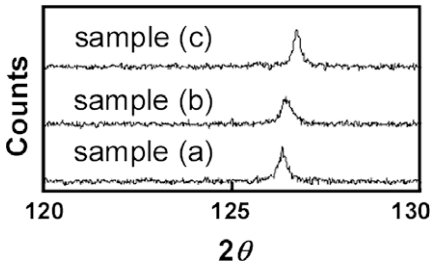

Fig. 2. XRD patterns for the samples annealed at 1973 K for 2 h and in various oxygen potentials: (a) −460 kJ/mol, (b) −405 kJ/mol, and (c) −360 kJ/mol.

Table 2
Lattice parameters and O/M ratios.

Sample	Oxygen potential (kJ/mol)	Lattice parameter (Å)	O/M
(a)	−435	5.460	1.95
(b)	−405	5.456	1.97
(c)	−360	5.450	1.99

Fig. 3 shows optical micrographs for samples (a), (b), and (c). In the micrographs, the MOX phase appears as a bright area and the pores are dark areas. The gray phase is present at grain boundaries of the MOX phase and the MOX grains have a round shape in samples (a) and (b). Thus the gray phase is a small amount of solute in the matrix phase. It is considered that the gray phase observed at grain boundaries is present as a liquid phase during annealing at 1973 K and the gray phase is SiO_2 phase, because SiO_2 is a liquid above 1973 K. In contrast, such a gray liquid phase does not appear at grain boundaries but at pores of the MOX phase in sample (c) having the highest O/M ratio.

The EPMA elemental mappings for samples (a–c) are shown in Fig. 4. The intensities of U and Pu signals are high in the same area of these maps, because the MOX consists of uranium oxide and plutonium oxide. In samples (a) and (b), some Si atoms are observed to coexist with Pu at MOX grain boundaries. In contrast, it can be seen that the SiO_2 phase is present at the pores of the MOX phase in sample (c). Behavior of SiO_2 observed in EPMA maps is the same as that of the gray phase observed in Fig. 3. Therefore, gray phase observed in Fig. 3 was confirmed to be SiO_2 phase. Fig. 5 shows the area fraction of SiO_2 and (Pu,Si)O in samples (a–c) annealed at 1973 K as a function of oxygen potential. This figure was based on the data of EPMA mappings of these samples. Here, in the case of coexistence of (Pu,Si)O with SiO_2, the area is regarded as (Pu,Si)O phase because (Pu,Si)O phase cannot be distinguished from SiO_2 due to resolution limits of the EPMA equipment. It is found that the area fraction of SiO_2 decreases but the (Pu,Si)O phase increases with decreasing oxygen potential. The SiO_2 phase at pores of the MOX phase such as observed in Fig. 3(c) is considered to form (Pu,Si) compound with decreasing oxygen potential.

3.2. Microstructure observation after annealing at temperatures between 1973 and 2673 K

Fig. 6 shows SEM micrographs for the samples with different O/M ratios after annealing at three different temperatures, 1973,

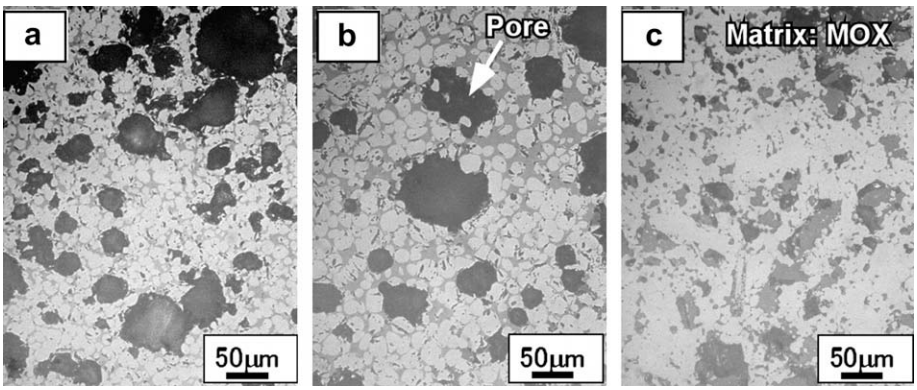

Fig. 3. Optical micrographs for samples having different O/M ratios after annealing at 1973 K for 2 h: (a) O/M = 1.95, (b) 1.97, and (c) 1.99.

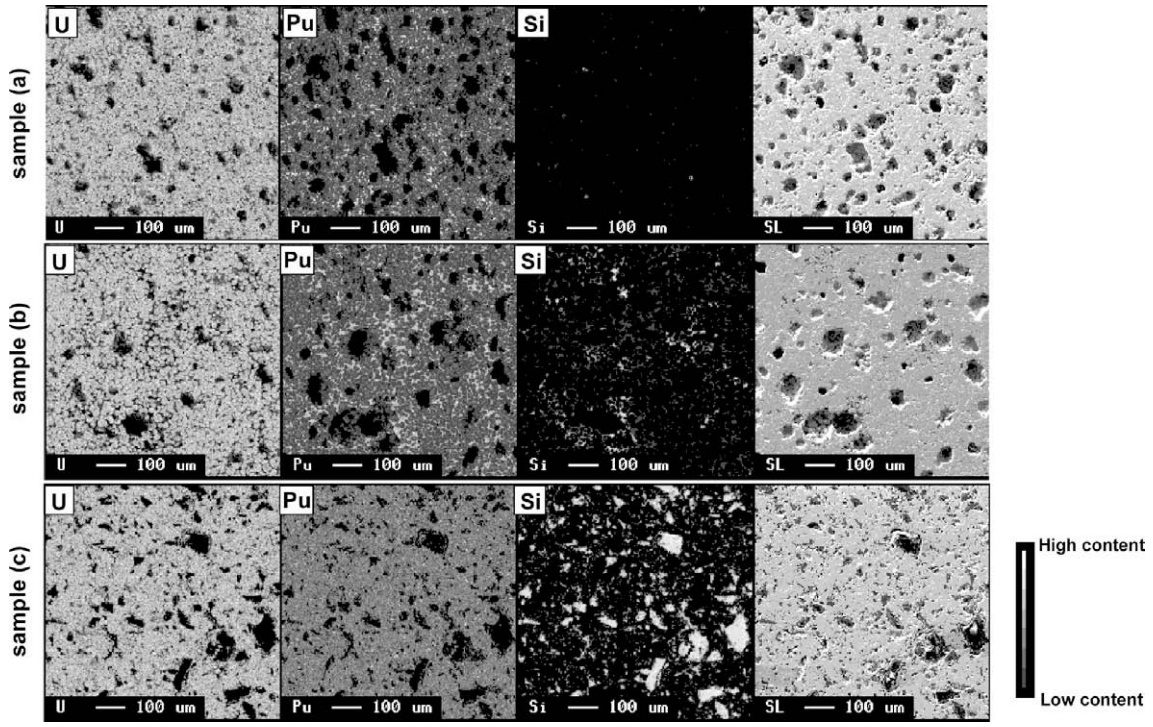

Fig. 4. EPMA mapping images of samples having different O/M ratios after annealing at 1973 K for 2 h: (a) O/M = 1.95, (b) 1.97, and (c) 1.99.

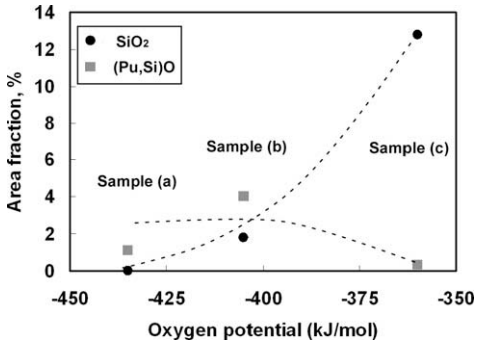

Fig. 5. Area fraction of SiO_2 phase and (Pu,Si)O phase in samples after annealing at 1973 K for 2 h as a function of oxygen potential.

2273, and 2673 K. The SiO_2 phase, which appears as dark in color in these micrographs, is observed predominantly at the pores of the MOX parent phase in sample (c) with the O/M ratio of 1.99 annealed at 1973 K (Fig. 6(c)). Micrographs for samples (a) and (b), in which the SiO_2 phase seems to be present as a liquid phase during annealing, reveal a lamellar phase at the grain boundaries of the MOX phase. From the results shown in Fig. 4, it is considered that the lamellar phase observed at grain boundaries in samples (a) and (b) is composed of a (Pu,Si) compound and SiO_2.

Fig. 6(d), (e), and (f) represent the microstructure in the samples annealed at 2273 K for 5 min. Because the grains possess round shapes, SiO_2 may have been present as a liquid phase during their annealing. In addition, Fig. 6d reveals that a lamellar phase, which is probably (Pu,Si) compound and SiO_2, is present at the grain boundaries. The microstructures of the samples annealed at 2673 K for 5 min are displayed in Fig. 6g, h, and i. These micrographs also suggest that SiO_2 is present as a liquid phase at grain boundaries of the MOX phase during annealing. It is found that the grain boundaries are single phase in samples (g) and (h) in contrast with samples (a), (b) and (d) which have the lamellar phase.

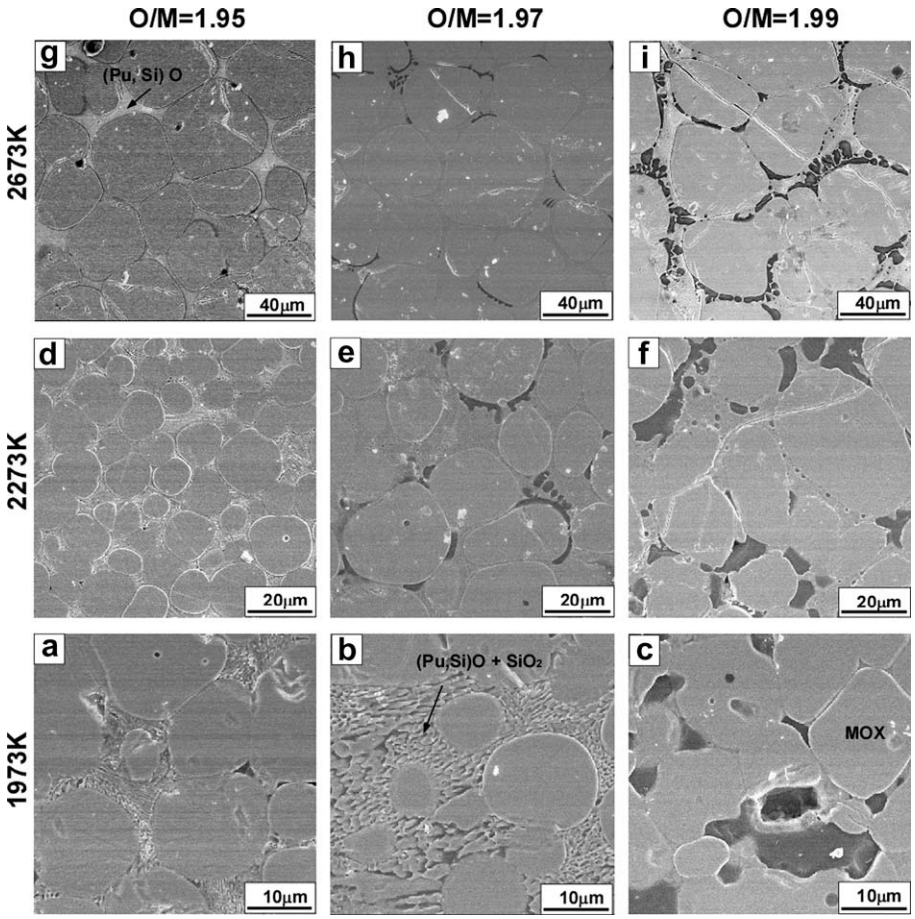

Fig. 6. SEM micrographs for samples annealed at three temperatures. Figure letters correspond to the sample identification letters.

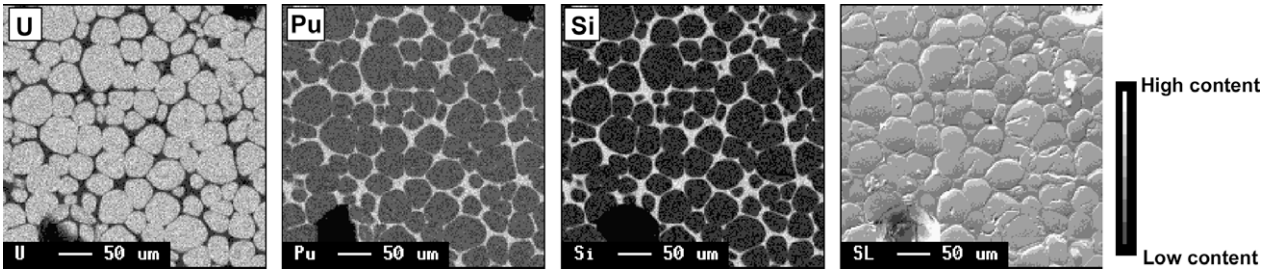

Fig. 7. EPMA elemental maps of sample (g).

Fig. 7 shows the EPMA elemental mappings for sample (g) annealed at 2673 K for 5 min. The mapping images reveal a noticeable difference between chemical distributions in this sample and those in other samples shown in Fig. 4. It is observed that Si distributes along grain boundaries of the MOX parent phase, and that Pu is enriched in the grain boundary phase. EPMA line-profiles from sample (g) are shown in Fig. 8. The line-profiles along A–A' indicate that Pu and Si are enriched at MOX grain boundaries. Moreover, the mol fraction of Pu to Si is the same at all grain boundaries. Therefore, the grain boundary phase consisting of Pu and Si in sample (g) is considered to be single phase.

It is known that compounds composed of Pu and Si are in the forms of $Pu_8(SiO_4)_6$ and $Pu_{9.33}(SiO_4)_6O_2$ containing Pu^{3+}, and $PuSiO_4$ containing Pu^{4+} [11,12], and the ratios of Pu to Si for these compounds are about 1.33, 1.56, and 1.00, respectively, in mol fraction. In the present work, the Pu to Si ratio is about 1.5 in mol fraction for sample (g) annealed at 2673 K for 5 min. The ratio obtained is close to the value for the compounds containing Pu^{3+}. Moreover, observable (Pu,Si) compounds tend to be formed in greater amounts with decreasing O/M ratio of MOX phase and with increasing annealing temperature. The valence of Pu in MOX is four with the O/M ratio of 2.00 and it changes to three with decreasing O/M ratio. In view of these points, it is considered that the compound observed at the grain boundaries is be either $Pu_8(SiO_4)_6$ or $Pu_{9.33}(SiO_4)_6O_2$.

3.3. Phase diagram of the MOX–SiO_2 system

In this section, the phase diagram in the MOX–SiO_2 system is discussed as a function of O/M ratio on the basis of the results of this work. It is necessary to discuss matrix phase separately from grain boundary phase, because matrix phase seems to be stable

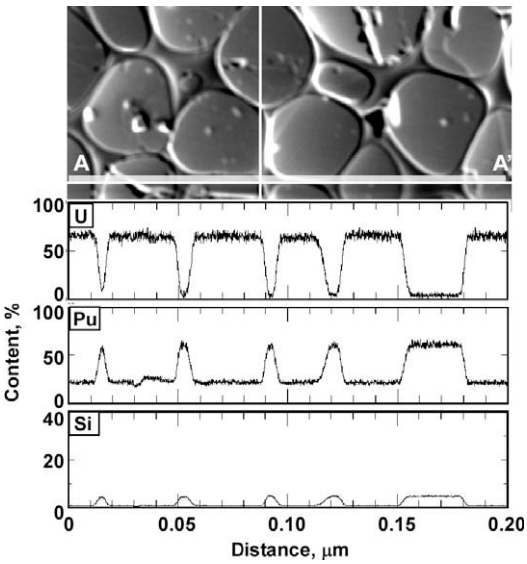

Fig. 8. EPMA line analysis of sample (g). The line analysis was carried out along the line A–A′ shown in the upper micrograph of this figure.

in all samples in this work but grain boundary phase changes with O/M ratio of each sample and the annealing temperature.

3.3.1. Matrix phase of the MOX–SiO_2 system

It is considered that the matrix phase of the MOX–SiO_2 system is MOX single phase because Si element cannot be observed in the MOX phase from EPMA mapping. In addition, the MOX phase is considered as a solid phase in this work. If the MOX parent phase could be melted even partly during heating, the grain size would be finer than that of the sample before annealing because the fine grains are developed during the solidification process. However, as can be seen in the samples annealed at 2273 K and 2673 K in Fig. 6, the grain sizes of these samples are larger than those of samples annealed at 1973 K.

3.3.2. Grain boundary phase of the MOX–SiO_2 system

It is expected that the grain boundary phase is composed of either (Pu,Si)O single phase, SiO_2 single phase or a mixture of (Pu,Si)O phase with SiO_2 phase.

Area fractions of SiO_2 and (Pu,Si)O are plotted as a function of O/M ratio on the basis of the data of EPMA mappings of each sample: fractions for samples (a–c) annealed at 1973 K are shown in Fig. 9, those of samples (d–f) annealed at 2273 K are in Fig. 10 and those of samples (g–i) annealed at 2673 K are in Fig. 11. Discussions on

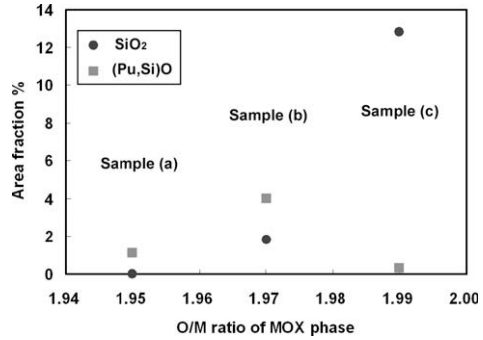

Fig. 9. Area fraction of SiO_2 phase and (Pu,Si)O phase in samples after annealing at 1973 K for 2 h as a function of O/M ratio.

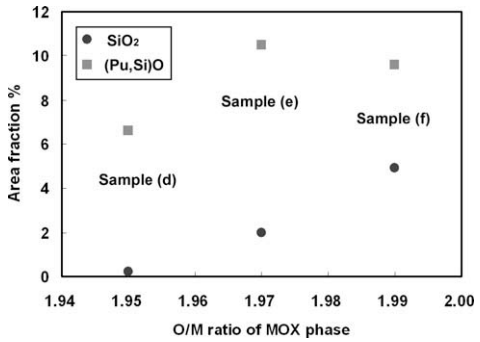

Fig. 10. Area fraction of SiO_2 phase and (Pu,Si)O phase in samples after annealing at 2273 K for 5 min as a function of O/M ratio.

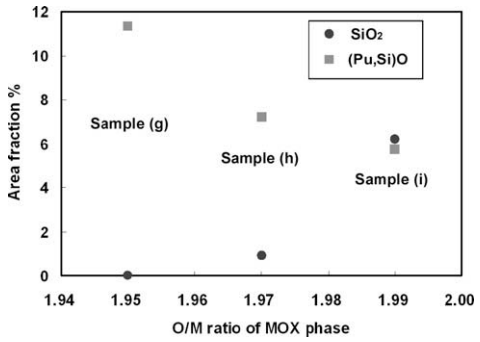

Fig. 11. Area fraction of SiO_2 phase and (Pu,Si)O phase in samples after annealing at 2673 K for 5 min as a function of O/M ratio.

the phase state of the grain boundary of each sample are given below and the phase state of samples is summarized in Table 3.

In the case of sample (a), SiO_2 phase does not seem to be present, and the grain boundary is composed of (Pu,Si)O single phase from the analysis of Fig. 9. As mentioned in Section 3.1, it is difficult to distinguish (Pu,Si)O phase from SiO_2 completely due to the limit in resolution of the EPMA equipment. The coexisting area of (Pu,Si)O with SiO_2 is regarded as (Pu,Si)O phase in this work. It is considered that grain boundary phase of sample (a) is two phases composed of (Pu,Si)O and SiO_2 because of the lamellar phase observed at the grain boundaries in the micrograph of Fig. 6(a).

Grain boundary phase of sample (b) is two phases composed of (Pu,Si)O and SiO_2 from the results of Fig. 9. It can also be confirmed that the boundary is two phase, because the lamellar microstructure is observed in Fig. 6(b).

As regards sample (c), the grain boundary phase is SiO_2 single phase from the results of Fig. 9.

Table 3
Phase state of matrix and grain boundary of samples during annealing in MOX–SiO_2 system.

Sample	Matrix phase	Grain boundary phase
(a)	MOX	(Pu,Si)O + SiO_2
(b)		(Pu,Si)O + SiO_2
(c)		SiO_2
(d)		(Pu,Si)O + SiO_2
(e)		(Pu,Si)O + SiO_2
(f)		(Pu,Si)O + SiO_2
(g)		(Pu,Si)O
(h)		(Pu,Si)O
(i)		(Pu,Si)O + SiO_2

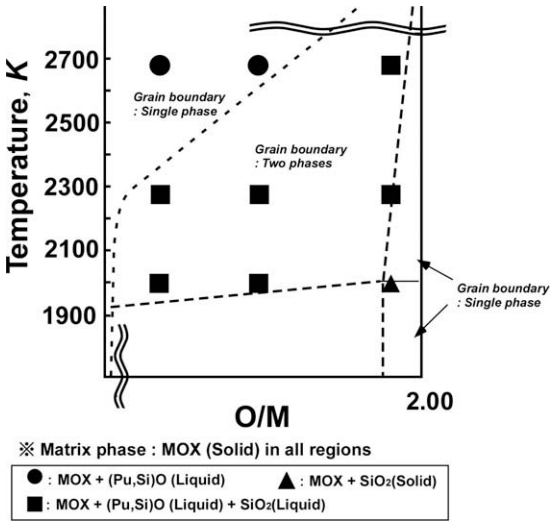

Fig. 12. MOX–SiO_2 system as a function of O/M ratio.

Grain boundary of sample (d) seems to be composed of (Pu,Si)O single phase from the analysis of Fig. 10. But as mentioned in discussing sample (a), the grain boundary phase is two phases composed of (Pu,Si)O and SiO_2 as lamellar phase at the grain boundary can be observed in the micrograph of Fig. 6(d).

In samples (e) and (f), the grain boundary phase is also two phases composed of (Pu,Si)O and SiO_2 the same as sample (d) from the results of Fig. 10.

In the case of sample (g), the boundary phase is (Pu,Si)O single phase from the results of Fig. 11. Single phase microstructure can also be confirmed from the micrograph of Fig. 6(g).

In the comparison with sample (g), the grain boundary phase of sample (h) seems to be two phases composed of (Pu,Si)O and SiO_2 from the results of Fig. 11. But the lamellar microstructure cannot be observed in the micrograph of Fig. 6(h). Therefore, it is considered the boundary phase is (Pu,Si)O single phase in this sample.

The grain boundary phase of sample (i) is two phases composed of (Pu,Si)O and SiO_2 from the results of Fig. 11.

Taking these results into consideration, a phase diagram of the MOX–SiO_2 system as a function of the O/M ratio of the MOX phase is proposed in Fig. 12. Borders between two phases are represented by broken lines. The black circles, squares and the triangle represent MOX + (Pu,Si)O(L), MOX + (Pu,Si)O + SiO_2(L) and MOX + SiO_2(S), respectively, and L and S within the parentheses, are liquid and solid phases, respectively. The compounds composed of Pu and Si are observed in almost all samples in this work. They are formed more observably with decreasing O/M ratio of the MOX phase and with increasing annealing temperature. However, the shapes of samples, which contain 25% SiO_2, are retained after heating at 2673 K. It is found that MOX phase is not affected significantly by Si impurity in this work.

4. Conclusions

The phase state of the MOX–SiO_2 system was studied as a function of oxygen-to-metal (O/M) ratio. (Pu,Si) compounds with other elements were observed along the grain boundaries of the MOX phase in samples after annealing. These compounds tended to form more observably with decreasing O/M ratio and with increasing annealing temperature. These compounds were not observed in the grain interior and the MOX matrix was not affected significantly by Si impurity presence.

References

[1] H. Funasaka, M. Itoh, in: Proceedings of Global 2007, Boise, Idaho, USA, September 9–13, 2007, pp. 259.
[2] K. Maeda, S. Sasaki, M. Kato, Y. Kihara, Plutonium Futures – The Science 2008, Dijion, France, July 7–11, 2008.
[3] K. Maeda, S. Sasaki, M. Kato, Y. Kihara, in: Symposium N of the EMRS Spring Meeting 2008, Strasbourg, France, May 26–30, 2008.
[4] K. Une, M. Hirai, K. Nogita, T. Hosokawa, Y. Suzawa, S. Shimizu, Y. Etoh, J. Nucl. Mater. 278 (2000) 54.
[5] S. Lungu, J.L. Beleuta, J. Nucl. Mater. 35 (1970) 35.
[6] J.J. Carbajo, G.L. Yoder, S.G. Popov, V.K. Ivanov, J. Nucl. Mater. 299 (2001) 181.
[7] K. Morimoto, M. Kato, M. Ogasawara, M. Kashimura, J. Nucl. Mater. 374 (2008) 378.
[8] E.A. Aitken, S.K. Evans, AEC Research and Development Report GEAP-5672, 1968.
[9] M. Kato, K. Morimoto, H. Sugata, K. Konashi, M. Kashimura, T. Abe, J. Alloys Compd. 452 (2008) 48.
[10] S. Kashibe, K. Une, J. Nucl. Mater. 254 (1998) 234.
[11] I.B. de Alleluia, Doctoral thesis, University of Karlsruhe, KFK-2849, 1979.
[12] C. Keller, Nukleonik 5 (1963) 41.